

## Identifying contact effects in electronic conduction through buckyballs on silicon

G.-C. Liang and A. W. Ghosh

School of Electrical and Computer Engineering, Purdue University, West Lafayette, IN 47907

We present a theory of current conduction through buckyball ( $C_{60}$ ) molecules on silicon by coupling a density functional treatment of the molecular levels embedded in silicon with a non-equilibrium Green's function (NEGF) treatment of quantum transport. Several experimental variations in conductance-voltage ( $G$ - $V$ ) characteristics are quantitatively accounted for by varying the detailed molecule-silicon bonding geometries. We identify how variations in contact surface microstructure influence the number, positions and shapes of the conductance peaks, while varying separations of the scanning probe from the molecules influence their peak amplitudes.

PACS numbers: PACS numbers: 05.10.Gg, 05.40.-a, 87.10.+e

Molecular electronics represents an ultimate dream for nanoscale material and device engineering. A long with well characterized, reproducible experiments, quantitative models for molecular conduction are crucial for a proper understanding and benchmarking of this emerging field, and for the exploration of novel device paradigms. A persistent problem has been incomplete knowledge of metal contact microstructures and their influence on conduction. In this respect, a semiconducting substrate provides a superior test-bed due to its well studied surface chemistry for transport measurements [1, 2]. It is therefore worthwhile to develop and refine our knowledge base using a familiar molecule bonded on a well-characterized silicon substrate that leaves little wiggle room for theory.

Among various molecules probed using scanning tunneling spectroscopy (STS), buckyball ( $C_{60}$ ) molecules stand out for their unique well calibrated bandstructure, alkali metal doped superconductivity, switching and optoelectronic properties [3]. Although STS studies of buckyballs on metals have allowed detailed comparison with theory [4], they do not reveal much information about their underlying contact microstructure. In contrast, buckyballs on silicon exhibit considerable variation in their  $G$ - $V$  characteristics depending on the nature of their covalent bondings with the surface dimers [5, 6, 7, 8].

In this paper, we explore conduction through buckyballs on silicon, and correlate observed variations in their  $G$ - $V$ s with variations in their contact bonding geometries (Fig. 1). A variation in the nature of the molecule-substrate bonding leads to a variation in the number and shapes of conductance peaks, while a variation in the tip-sample tunneling gap leads to a variation in the relative peak heights. Our theoretical formulation thus serves a dual purpose: on one hand, it tests our quantitative model for molecular conduction, in particular on a sophisticated semiconducting substrate; on the other hand, it provides useful insights that allow us to deconstruct the role of contact geometry on molecular conduction.

Theoretical technique. We calculate molecular conduction by coupling an electronic structure calculation for the molecule and the contacts with a treatment of quan-

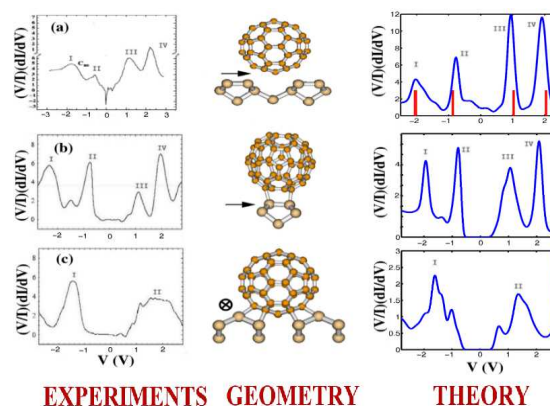


FIG. 1: Different STS measurements [5, 6] on  $C_{60}$  molecules docked onto Si(100)  $2 \times 1$  surface (left panel). We attribute different bonding geometries (middle panel) for each experiment, leading to a theoretical  $G$ - $V$  (right panel) that agrees quite well with the corresponding measurement. The arrow represents the dimer direction of the reconstructed surface (cross going into the page). The upper geometry corresponds to  $C_{60}$  physisorbed on four surface dimers, the middle one represents the buckyball chemically bonded with a single surface dimer, while the bottom one has the molecule lowered into the trough caused by a missing dimer.

tum transport using NEGF [9, 10]. The  $C_{60}$  structure and Hamiltonian are obtained using density functional theory within the local density approximation (LDA). The reconstructed surface geometry of Si(100) is obtained by LDA optimization with a norm-conserving pseudopotential in a plane-wave basis [11]. Although it is possible in principle to describe the silicon bandstructure using DFT, as has been customarily done in the past for metal substrates [10, 12], adapting the same process to semiconductors is quite challenging, given the complicated bandstructure, extended band-bending and incomplete screening, reconstruction, and surface chemistry of silicon. Fortunately, within the NEGF formalism one can formally partition the problem so that the only quantum effect of the silicon substrate that the molecule

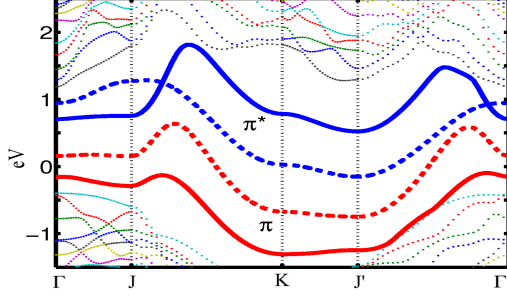


FIG. 2: Calculated surface bandstructure of asymmetric dimer (solid lines) and symmetric dimer (dashed lines) reconstructions along Si(100)-2x1 using EHT bulk Si parameters [14] and optimized surface geometries [11].

is sensitive to residues in its surface Green's function. In the past, we developed a technique for combining different electronic structure codes by matching their interfacial Green's functions expressed in two different atomic basis sets. The match is exact for two equally complete basis sets and a best-otherwise, and only assumes local separability of their one-electron potentials [2, 13].

We use an Extended Huckel (EHT) type model parametrized by Cerda et. al. [14] to generate a good quantitative description of the bulk silicon bandstructure (calibrated with LDA+GGA calculations), and also the surface band structure of 2x1 reconstructed Si-(100) (calibrated with experiments and GGA calculations [15]). To check the properties of Si(100)-2x1 reconstructed surface properly, a slab of 13 silicon layers with a hydrogen-passivated bottom layer is used to simulate the bandstructure of Si(100)-2x1 asymmetric dimer (AD) reconstruction and symmetric dimer (SD) reconstruction. The red and blue solid lines in Fig 2 represent the  $\pi$  and  $\pi^*$  states of Si(100)-2x1 AD reconstruction while the dashed lines represent the corresponding  $\pi$  and  $\pi^*$  states of the SD reconstruction. The former clearly shows a bandgap

0.6 eV while the latter shows a continuum of states in the bulk bandgap region. After benchmarking these properties (details will be published elsewhere), the recursive surface green's function is computed for the semi-infinite silicon substrate. We then use a mixed-basis method [13] to transfer the Si(100) surface Green's function computed in the EHT Slater type orbital (STO) basis into a 6-31g(d) basis set that is then connected with a DFT/6-31g(d) Hamiltonian for the molecule.

While the molecule and substrate are modeled atomistically, we employ a simpler treatment of the STM tip using a self-energy  $\Sigma_2(d_0)$  [2], where  $d_0$  is the tip to molecule bond length. More sophisticated models could be used to describe tip-sample interactions in experiments with well characterized tip structures. Vacuum tunneling is described using a typical WKB factor [16]

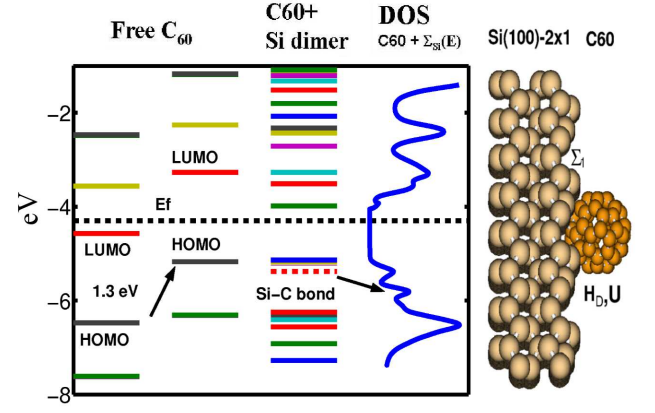


FIG. 3: Energy level alignment between  $C_{60}$  and silicon. The left panel shows the energy levels of isolated  $C_{60}$ , with the calculated Fermi energy of the doped silicon shown as a dashed line. The  $C_{60}$  energy levels are shifted by 1.3 eV due to self-consistent charging driven by the workfunction difference between the molecule and the substrate, and the corresponding charge transfer from Si to  $C_{60}$ . Chemisorption creates new levels due to Si-C bonds, easily seen by adding a silicon dimer to the molecule and passivating the cluster at the bottom. Finally, including the silicon self-energy amounts to adding the entire silicon substrate and generates a continuum molecular band. The right panel shows the density of states corresponding to the geometry in the middle of Fig. 1.

premultiplying  $\Sigma_2(d_0)$ , making the net self-energy  $\Sigma_2$  energy and distance dependant. Our approach includes the bias-dependent barrier profile and agrees quantitatively with measured STS spectra on bare silicon.

Equilibrium band diagram. We start by describing the silicon-buckyball bonding chemistry, band formation, and the corresponding band alignment due to charge transfer. DFT (LSDA/6-31g) gives a good description of the energy levels for isolated  $C_{60}$ . The highest occupied molecular orbital (HOMO) is at -6.5 eV while the lowest unoccupied molecular orbital (LUMO) is at -4.6 eV relative to vacuum. Once the buckyball connects to n-doped silicon, electrons are transferred from Si to  $C_{60}$  because the Fermi level of Si is higher than the  $C_{60}$  LUMO. Self-consistent calculations with a Hubbard-type capacitive charging energy [18] yield a net charge transfer that raises the energy levels of  $C_{60}$  by about 1.3 eV, which is very close to the difference in workfunction between  $C_{60}$  and Si. The charging energy of the Hubbard Hamiltonian [19] is chosen to be 1.2 eV, consistent with experiments involving  $C_{60}$  on metal and with solid  $C_{60}$  surface [20].

Fig. 3 explains the energy level diagram using the geometry in the middle of Fig. 1 as an example. The solid lines represent the energy levels of an isolated buckyball, while the dashed line represents the Fermi level of bulk Si calculated from the experimental doping levels [5]. In addition to the charge transfer and band-alignment driven by electrostatics, there is also substantial transfer

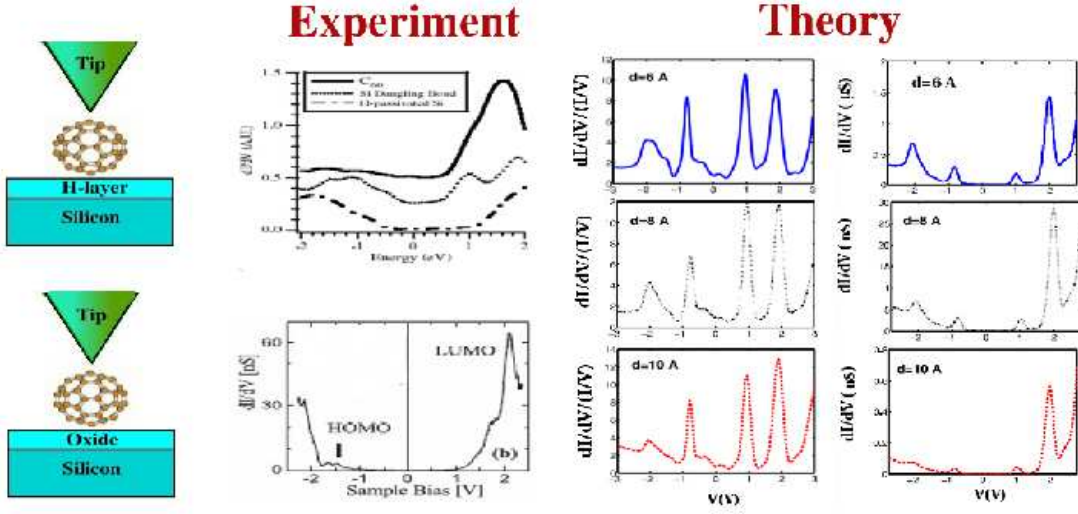


FIG. 4: Introducing tunnel barriers between the STM and the sample or the sample and the substrate (far left) de-emphasizes the HOMO levels relative to the LUMO ones due to their relatively larger barrier heights, accounting for measurements (left) with little or no signature of HOMO levels [7, 8]. Although the unnormalized conductance shows this effect with increasing tip-sample separation  $d$  (right), normalizing the conductance (center) as in Fig. 1 restores these peaks.

of spectral weight from Si to  $C_{60}$  leading to the formation of bonding-antibonding pairs. The energy levels of  $C_{60}$  bonded with a single surface silicon dimer system shows the effect of bonding, which leads to both level rearrangement and level creation. A wave-function plot of those levels shows a lot of hybridization between C and Si. The rightmost panel shows the density of states of  $C_{60}$  with the Si surface which provides the proper boundary conditions of the open system described with an energy-dependent self-energy. A clear peak appears between the HOMO and HOMO-1 levels in the STS (i.e., between peaks marked I and II), which we attribute to the Si-C bond arising from strong Si and C hybridization.

**Results: Peak positions and heights.** Fig. 1 shows the calculated  $G-V$ s for  $C_{60}$  docked on a clean silicon surface with different bonding geometries. The conductances are normalized using an averaging procedure adopted in the experimental analyses [21, 22]. The upper set of figures corresponds to  $C_{60}$  physisorbed on the Si(100)-2 $\times$ 1 surface. The bottom of the buckyball is kept 2.1 Å away from the Si surface dimer to ensure weak coupling. Under these circumstances, the STS probes the bare  $C_{60}$  electronic structure with the molecular levels (Fig. 3) generating  $G-V$  peaks marked I, II, III, and IV in Fig. 1. The vertical bars in Fig. 1 denote the LDA/4-31g HOMO-1, HOMO, LUMO, and LUMO+1 levels of isolated  $C_{60}$  rigidly shifted by 1.2 eV due to charging as before, although the precise shift differs due to the different Fermi energies of the n and p-Si substrates. The excellent correspondence between the isolated  $C_{60}$  levels and the conductance peaks thus gives us an elementary interpretation of the STS data in the upper geometry of Fig. 1.

The bonding geometry between  $C_{60}$  and the Si(100)

surface changes upon annealing from physisorption to chemisorption [23], corresponding to the middle and the bottom sets of plots in Fig. 1. We consider two prominent chemisorption geometries based on experimental suggestions. The first consists of  $C_{60}$  chemically bonded with a Si surface dimer that straddles diametrically opposite ends of a  $C_{60}$  hexagon. The experimental  $dI/dV/(I/V)$ s measured using STS are reproduced by our density functional conductance calculation, with the only variable being the geometry itself. The four main marked peaks still arise from the isolated  $C_{60}$  energy levels discussed above. In addition, our calculation reveals an extra smaller peak between peaks I and II, as in the experiments. This small peak has also been observed by ultraviolet photoemission spectroscopy (UPS) measurements on the  $C_{60}/Si(100)-2\times 1$  system [24]. The origin of this secondary peak is from strong covalent Si-C bonding, seen in the correlation diagram between  $C_{60}$  and a surface Si dimer in Fig. 3 and also in the corresponding density of states.

The bottom plot of Fig. 1 shows the experimental and calculated conductances corresponding to a different chemisorption geometry realized upon annealing, consisting of a missing silicon dimer that causes the buckyball to drop into the empty trough [5]. It is clear from the bonding geometry (middle panel), that the closer proximity with the surface leads to the establishment of more covalent bonds, radically altering the electronic structure of bare  $C_{60}$ . The STS  $G-V$  in (c) is qualitatively different from the geometries in (a) and (b). There is one clear HOMO peak for negative substrate bias and a broadened LUMO level in the positive direction replacing the four original peaks. Our simulation captures the main features of this experiment. The original Si-C peak



goes up to become the main negative bias peak, while several additional SiC peaks are formed near the conducting LUMO levels due to the additional bondings. In addition, our calculation generates spurious peaks from the unrelaxed  $C_{60}$  structure adopted in our calculation for convenience. We believe that strong chemisorption would deform the  $C_{60}$  near the bottom, eliminating these extra peaks by bonding-antibonding splitting. We leave a detailed study of  $C_{60}$  relaxation for future work.

In addition to the number and positions of the peaks, other experiments show variations in the conductance peak heights [6, 7, 8] (Fig. 4). A possible origin is the differing tip-sample spacings in these experiments. A WKB treatment of tunneling through varying vacuum thicknesses provides a qualitative explanation. Using the physisorbed geometry in Fig. 1(a) as an example, we find that increasing the tip-sample gap from 6 Å to 8 Å and then to 1 nm progressively deemphasizes the role of the HOMO levels in comparison to the LUMO levels. Note however that such WKB factors are eliminated in the earlier log-normalized  $dI/dV / (I/V)$  plots (Fig. 4), as expected [21] but show up in the unnormalized  $dI/dV$  conductance plots (Fig. 4). From the  $dI/dV$  vs  $V$  in Fig. 4, it is very clear that the thicker barrier cuts down the HOMO contributions exponentially to within the noise levels of the experiment. Electrons tunneling from the HOMO level in the negative bias direction encounter a higher tunneling barrier than electrons from the STM

lining the LUMO higher up. The WKB approximation suggests that each peak height is reduced roughly in proportion to  $\exp(-2kd)$  where  $k$  represents the decay constant of the corresponding level and  $d$  is the tip-sample separation. We therefore believe that measurements with no clear HOMO peaks are performed with an STM tip substantially removed from the molecule. Furthermore, the experiments in Fig. 4 have an extra tunneling barrier between the molecule and the substrate (a hydrogen passivation layer in the top example and an oxide layer in the bottom [25]). This additional barrier would further deemphasize the HOMO contributions, practically eliminating them from the unnormalized conductance curves.

In summary, we have used  $C_{60}$  on silicon to demonstrate our capacity to theoretically deconstruct the role of contact microstructure on molecular conduction. The unexplained features are the peak broadenings, which should depend on coupling with the dimer and the molecular vibrational modes. A treatment of vibronic scattering would indeed be worth pursuing both for its exciting physics and for further benchmarking between experimental and computational molecular conduction.

We thank S. Datta, M. Lundström, T. Rakshit, D. Kienle and M. Hersam for useful discussions. This project has been supported by ARO-DURINT, DARPA, SRC and NCN.

- [2] T. Rakshit, G.-C. Liang, A. W. Ghosh, and S. Datta, *Nano Letters*, 4 1803 (2004).
- [3] M. S. Dresselhaus, G. Dresselhaus and P. C. Eklund, *"Science of Fullerenes and Carbon Nanotubes"* Academic Press (1996).
- [4] Xinghua Lu, M. Gobis, K. H. Khoo, Steven G. Louie, and M. F. Crommie, *Phys. Rev. B* 70 115418 (2004).
- [5] X. Yao, T. G. Ruskell, R. K. Workman, D. Sarid and D. Chen, *Surface Science* 366 L743 (1996); X. Yao, R. K. Workman, C. A. Peterson, D. Chen and D. Sarid, *Applied Physics A* 66 S107 (1998).
- [6] A. W. Dunn, E. D. Svensson and C. Dekker, *Surface Science* 498 237 (2002).
- [7] M. C. Hersam, N. P. Guisinger and J. W. Lyding, *Nanotechnology* 11 70 (2000).
- [8] L. Bolotov, N. Uchida, and T. Kanayama, *Journal of Physics*, 15 S3065 (2003).
- [9] S. Datta, *"Electronic transport in mesoscopic systems"* Cambridge University Press (1995).
- [10] P. Damle, A. W. Ghosh, and S. Datta, *J. Chem. Phys.* 117, 281 (2002).
- [11] A. Ramstad, G. B. Rocks, and P. J. Kelly, *Phys. Rev. B* 51 14504 (1995).
- [12] M. Brandbyge, J.-L. Mozos, P. Ordejón, J. Taylor, and K. Stokbro, *Phys. Rev. B* 65, 165401 (2002).
- [13] A. W. Ghosh, unpublished.
- [14] J. Cerda and F. Soria, *Phys. Rev. B* 61 7965 (2000).
- [15] M. Rohlfing, P. Krüger, and J. Pollmann, *Phys. Rev. B* 52 13573 (1995).
- [16] L. Perdigão, D. Dreesen, B. G. Randier, M. Dubois, C. Delenne, G. Allan, and D. Stievenard, *Physical Review Letters* 92, 216101 (2004).
- [17] T. Rakshit, G.-C. Liang, A. W. Ghosh and S. Datta, unpublished.
- [18] We have used a simple model for self-consistency since the tips are far from the molecule so that the voltage drops mainly across the tip-sample gap and the molecular potential stays tied to the substrate. Under these conditions, the transmission peak energies directly translate into peak voltages with no Laplace scaling factors. The strong substrate-molecule coupling keeps the molecule out of the Coulomb blockade regime, so that charging is adiabatic and the HOMO-LUMO gap stays unaffected.
- [19] P. Fulde, *"Electron correlations in molecules and solids"* Springer-Verlag 1991.
- [20] R. Hesper, L. H. Tjeng and G. A. Sawatzky, *Europhysics Letters* 40 177 (1997).
- [21] C. J. Chen, *"Introduction to Scanning and Tunneling Microscopy"* Oxford University Press, 1993.
- [22] D. Drid, *"Exploring Scanning Probe Microscopy with Mathematics"* John Wiley and Sons, INC (1997).
- [23] D. Chen and D. Sarid, *Surface Science* 329 206 (1995).
- [24] M. De Seta, D. Sanvitto, and F. Evangelisti, *Phys. Rev. B* 59 9878 (1999).
- [25] The HOMO-LUMO gap here is larger, possibly due to a voltage division factor that can be readily incorporated in our model.